JVSTA Journal of Vacuum Science & Technology A

Mechanistic modeling study on process optimization and precursor utilization with atmospheric spatial atomic layer deposition

Zhang Deng, Wenjie He, Chenlong Duan, Rong Chen, and Bin Shan

Citation: Journal of Vacuum Science & Technology A **34**, 01A108 (2016); doi: 10.1116/1.4932564
View online: http://dx.doi.org/10.1116/1.4932564
View Table of Contents: http://scitation.aip.org/content/avs/journal/jvsta/34/1?ver=pdfcov
Published by the AVS: Science & Technology of Materials, Interfaces, and Processing

Mechanistic modeling study on process optimization and precursor utilization with atmospheric spatial atomic layer deposition

Zhang Deng, Wenjie He, and Chenlong Duan
State Key Laboratory of Digital Manufacturing Equipment and Technology, School of Mechanical Science and Engineering, Huazhong University of Science and Technology, Wuhan, Hubei 430074, People's Republic of China

Rong Chen[a)]
State Key Laboratory of Digital Manufacturing Equipment and Technology, School of Mechanical Science and Engineering, School of Optical and Electronic Information, Huazhong University of Science and Technology, Wuhan, Hubei 430074, People's Republic of China

Bin Shan
State Key Laboratory of Material Processing and Die & Mould Technology, School of Materials Science and Engineering, Huazhong University of Science and Technology, Wuhan, Hubei 430074, People's Republic of China

(Received 12 August 2015; accepted 25 September 2015; published 6 October 2015)

Spatial atomic layer deposition (SALD) is a promising technology with the aim of combining the advantages of excellent uniformity and conformity of temporal atomic layer deposition (ALD), and an industrial scalable and continuous process. In this manuscript, an experimental and numerical combined model of atmospheric SALD system is presented. To establish the connection between the process parameters and the growth efficiency, a quantitative model on reactant isolation, throughput, and precursor utilization is performed based on the separation gas flow rate, carrier gas flow rate, and precursor mass fraction. The simulation results based on this model show an inverse relation between the precursor usage and the carrier gas flow rate. With the constant carrier gas flow, the relationship of precursor usage and precursor mass fraction follows monotonic function. The precursor concentration, regardless of gas velocity, is the determinant factor of the minimal residual time. The narrow gap between precursor injecting heads and the substrate surface in general SALD system leads to a low Péclet number. In this situation, the gas diffusion act as a leading role in the precursor transport in the small gap rather than the convection. Fluid kinetics from the numerical model is independent of the specific structure, which is instructive for the SALD geometry design as well as its process optimization. © *2015 American Vacuum Society*.
[http://dx.doi.org/10.1116/1.4932564]

I. INTRODUCTION

Atomic layer deposition (ALD) is an ultrathin film deposition technique. Relying on its self-terminating nature, ALD enables atomic level control over the film thickness.[1,2] In a typical ALD process, dosing and purging steps are implemented in an alternating sequence.[3–5] Only one kind of precursor resides in the reaction chamber in the dosing process, and then, the excess species are removed by the inert gas purging. Due to the temporal division of the dosing and purging steps, the film growth rate is relatively low at a level of approximately nanometers per minute.[6–10] As an alternative approach to temporal ALD, spatial ALD (SALD) is a promising technology with the aim of combining the advantages of uniformity and conformity, and a scalable process with high growth rates. Similar to temporal ALD, the primary requirement of the SALD is to separate the precursors effectively. Since the precursors are fed into the reactor simultaneously, it is important to optimize the process to avoid unnecessary long cycle times and the nonuniform deposition.

Researchers have conducted experimental studies on the SALD process with different parameters of reactor structure,[11–28] such as the reactor with the multiple slits gas head,[13–16] the rotating gas head[17–22] and the rolled substrate.[23–26] At present, the optimizations of the SALD process mainly rely on massive experiment runs.[26–28] Compared to temporal ALD system, SALD is more complicated since the multiple reactions and the substrate motion happen simultaneously. Considering all these challenges, equipment scale simulation becomes an important method to understand and establish the correlation among fluid parameters, structure dimensions, throughput, and precursor utilization. The numerical methods have already been utilized to analyze process parameters and enhance the understanding of physical and chemical processes.[29–33] Many numerical approaches incorporating both molecular scale with equipment scale calculations are devoted to study physical interactions and chemical kinetics of the ALD.[29,30] Yuan's group presents a numerical model which describes the temporal ALD process with the surface chemistry in equipment scale.[31–33] The SALD, however, is operated under a wide pressure range from vacuum to atmosphere with continuous precursors dosing and the substrate motion. Reports on the complicated correlation among fluid parameters, structure dimensions, throughput, and efficiency have been rarely discussed in the SALD system.

[a)]Electronic mail: rongchen@mail.hust.edu.cn

Numerical details of multiple species and reactions in our SALD model are studied to bridge the process conditions and growth efficiency. The separation gas flow, carrier gas flow, and precursor mass fraction are, respectively, studied for the quantitative correlation on reactant isolation, throughput, and precursor utilization. The intermixing of precursors at different separation gas flow rates is traced in the numerical model. The overall throughput is characterized by the precursor concentration, carrier gas flow and the minimal residual time. The monotonic function between precursor usage and precursor concentration in the SALD system is derived from the simulation results. Finally, the precursor transport in the narrow gap is characterized by the Péclet number.

II. EXPERIMENT

The growth of Al_2O_3 thin film at atmospheric pressure is performed on an SALD reactor shown in Fig. 1. The SALD system primarily consists of a multiple slits gas head unit and a moving substrate holder. The substrate holder translationally moves back-and-forth under the gas head. The gas head could be extended by adding a series of gas head units both horizontally and vertically, which is applicable to the large planar or curvature substrates. Precursors are stored in N_2-assisted bottles at room temperature (25 °C). Each precursor is taken out from the double-way bottle by highly pure nitrogen gas, and diluted with abundant nitrogen gas flow again before filling into the corresponding precursor channels. During the entire operations, precursors flux into the reactor with constant concentrations. The temperature of the moving substrate is set at 150 °C constantly.

From cross-sectional schematic diagram of the gas head unit shown in Fig. 1, the gas flow conditions, reactor dimensions, and substrate moving speed jointly impact the deposition process. From the perspective of precursor utilization, the relationship between surface reactants and precursor mass can be deduced from

$$\frac{A}{t} + v_{\text{substrate}} B \leq \frac{f\rho}{S}, \tag{1}$$

where both A and B are the constants related to molar mass of surface species, t is the reaction time in precursor channel, $v_{\text{substrate}}$ is the substrate moving speed, f is the carrier gas mass flow rate in the precursor channel, ρ is the precursor concentration, and S is the area of the precursor channel section. The substrate moving speed $v_{\text{substrate}}$, gas flow rate f, and precursor mass fraction ρ are discussed on throughput and precursor utilization of the SALD process.

III. MODELING

The computational fluid dynamics model is chosen to analyze fluid kinetics by solving the set of conservation equations for mass, momentum, and energy. A group of reactions is integrated into the conventional dynamic flow model of a continuous process, where the surface depositions and volume reactions take place simultaneously in the SALD process. Two surface reactions are shown in below Eqs. (a) and (b), respectively. The trimethylaluminum (TMA) and water are selected as precursors for two half surface reactions, and M- presents the surface species. When two precursor molecules meet in the space, the volumetric reaction presented in below Eq. (c) happens, and Al_2O_3 powder will be produced.

(a) $Al(CH_3)_3 + \text{M-OH} \rightarrow \text{M-O-Al}(CH_3)_2 + CH_4$,
(b) $2H_2O + \text{M-O-Al}(CH_3)_2 \rightarrow 2\text{M-O-Al-OH} + 2CH_4$,
(c) $2Al(CH_3)_3 + 3H_2O \rightarrow Al_2O_3 + 6CH_4$.

To combine multiple chemical reactions with species transport in the SALD process, the production rates in chemical reactions are calculated through the laminar finite-rate model using Arrhenius expression

$$R_i = M_i \sum_{i=1}^{N_r} \hat{R}_{i,r}, \tag{2}$$

where R_i and M_i are the production rate and molecular weight of reaction product i, respectively. $\hat{R}_{i,r}$ is the Arrhenius molar rate of creation or destruction of reaction product i in reaction r. The general form of the rth irreversible surface reaction in ALD takes the form as

$$\sum_{i=1}^{n_g} g_i' G_i + \sum_{i=1}^{n_s} s_i' S_i + \sum_{i=1}^{n_r} r_i' R_i \xrightarrow{k_r} \sum_{i=1}^{n_g} g_i'' G_i + \sum_{i=1}^{n_s} s_i'' S_i + \sum_{i=1}^{n_r} r_i'' R_i, \tag{3}$$

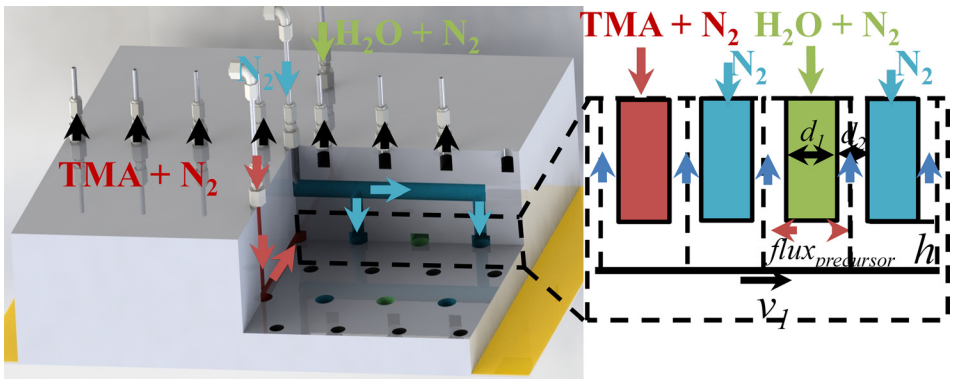

FIG. 1. (Color online) Structure of spatial ALD reactor and the cross-section schematic diagram of gas head unit.

where G_i, S_i, and R_i denote gaseous species, bulk (solid) species, and surface species, respectively; n_g, n_s, and n_r are the total numbers of the corresponding gaseous, bulk species, and surface species; g_i', s_i', and r_i' are the corresponding stoichiometric coefficients for each reactant; g_i'', s_i'', and r_i'' are the stoichiometric coefficients for each product; the rate constant k_r is evaluated by the Arrhenius expression.

Numerical simulation is implemented on the 3D domain with a nonstructural meshing scheme (Fig. 2) by the commercial solver package of ANSYS FLUENT. The fluid domain bases on the structure of multiple slits and rectangular channels.[16] The gas head is composed of a series of rectangular channels with dimensions of 45 mm (length) × 1.8 mm (width) × 0.5 mm (height). The exhaust channel and separation gas channel are separated by 1.0 mm from each other. The reactant channel and exhaust channel are positioned at an interval of 1 mm. Several cylinders with a diameter of 1.0 mm are designed at the top of the rectangular channel to provide the dispersed gas. The gap distance between gas head and moving substrate is maintained at 0.5 mm in continuous process. The reaction equations above are calculated combined with computational dynamics described in the Appendix. The laminar finite-rate method is chosen for surface reactions calculation in the SALD system. The second-order upwind method is selected for spatial discretization and approximation of the continuity equation, energy equation, and species transport equations. With finite volume method with a pressure–mass flow rate coupled scheme, the calculations are implemented at each domain node. The second-order implicit method is chosen for the time discretization. The second-order numerical method is chosen for sufficient computational accuracy.

IV. RESULTS AND DISCUSSION

A. Fluid kinetics details with numerical model

One important characteristic of the ALD process is the effective separation of different precursors to ensure self-limiting surface reaction. In the SALD system, keeping the isolation becomes more challenging since precursors are fed into the reactor simultaneously. As presented in Fig. 1, the positions of injecting channel of precursor, exhaust channel, injecting channel of separation gas, and another exhaust channel are arranged sequentially in one gas head unit. As Fig. 3(a) shows, carrier gas and precursors flow into the reactant channels in the direction perpendicular to the substrate movement. The carrier gas and the inert gas are fed into the deposition areas and barrier areas, respectively, forming a gas flow layer within the narrow gap between the lower surface of the gas head and the substrate. Precursor is diluted with the nitrogen gas, and fills into the corresponding reactant channels. In the narrow gap, the precursor molecules are transported into the gas flow layer and react with active species of the surface. The excess precursors are forced to flow into the adjacent exhaust channels. This zone between reactant channel and two adjoining exhaust channels is the reaction region. Inert gas flows from the separation channel into the gap, obstructs the diffusion, and then escapes from the exhaust channels. The isolation region as a "gas curtain" to barrier the intermixing is formed between two reaction regions. The substrate moves through reaction regions and isolation regions alternately. If there is a cross diffusion of precursors or ambient moisture in continuous process, the volumetric reaction in equation (c) will happen leading to uncontrollable growth of thin films.

Figure 3(b) shows the concentrations of three species (TMA, water, methane, respectively) with 1000 sccm separation gas flow rate, 200 sccm carrier gas flow rate and 1% TMA mass fraction at atmospheric pressure. Although there seems no cross diffusion of precursors in space judged by the TMA and water distributions, the byproduct of the reaction is measured in the TMA exhaust channels.

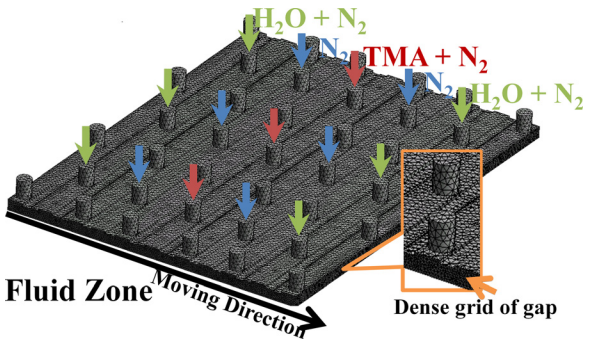

FIG. 2. (Color online) Three-dimensional computational domain with multiple slits in the numerical model.

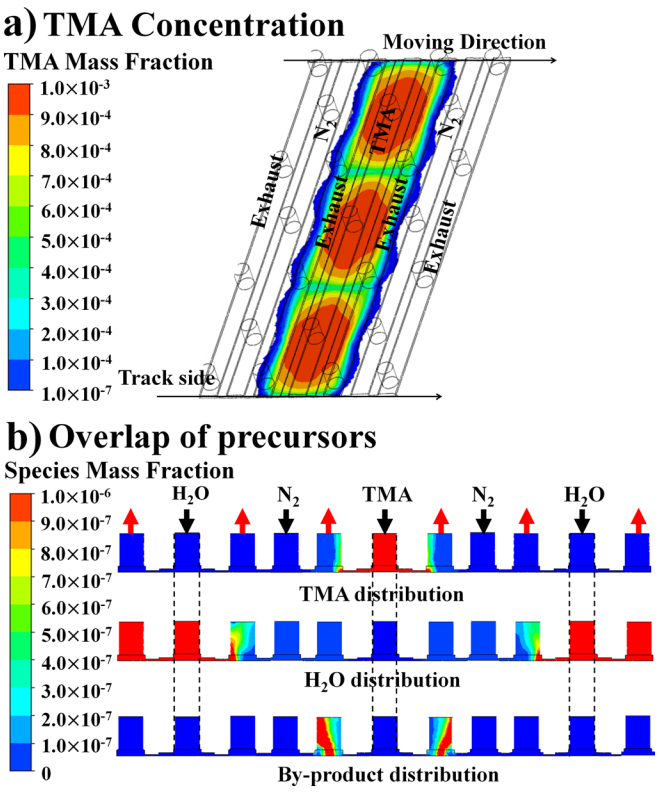

FIG. 3. (Color online) (a) Volumetric concentration of TMA in reaction channel and (b) the distribution of precursor molecules and detection of overlap at TMA exhausts in the continuous process with 1000 sccm separation gas flow, 200 sccm carrier gas flow, and 1% TMA mass fraction.

The concentration of byproduct methane is higher than 1 ppm (species mass fraction in gas mixture is 1.0×10^{-6}), indicating a high probability of precursors overlap. In experiments, after thousands of monolayer growth, some white powder can be observed at the exhaust channels or the ambient perimeter of the gas head which reveals the cross diffusion of precursors.[16] The cross diffusion from the experimental observations is in agreement with our simulation results, showing the validity of such a numerical model. More importantly, the quantitative calculation of byproduct could act as a sensitive indicator of cross diffusion if the byproduct mass fraction is below 1.0×10^{-9}. In addition, the location where high concentration of gaseous methane exists [at TMA exhaust channels in Fig. 3(b)] could accurately detect where the precursors intermixing happens.

B. Efficiency analysis of continuous process

1. Effective separation of precursor cross-diffusion

The cross diffusion of precursors or ambient moisture changes the film growth rate and causes uncontrollable growth. Therefore, effective separation of precursors is critical to assure the ideal ALD growth. When separation gas flow is large enough to reduce the precursor concentration lower than 1 ppm, there is almost no cross diffusion in continuous process. Experiments and simulations with 200–2000 sccm separation gas flows are conducted under atmospheric pressure to examine the separation. With 200 sccm carrier gas flow, the separation gas flow rate needs to be larger than 1000 sccm to separate the precursors from ambient moisture. The probability of cross diffusion increases if the separation gas flow is smaller than 1000 sccm. The precursor is taken from the double-way precursor bottle by 20 sccm nitrogen, and then diluted with 200 sccm nitrogen again before it finally fills into the corresponding injecting channels. The substrate keeps stationary when separation gas is fluxed continuously. The capillary probe of the *in situ* quadrupole mass spectrometer is located at the point of the substrate which is under the exhaust channel. The simulation results of methane concentration and separation gas flow rates in Fig. 4 agree well with the experiments. The experimental tolerance at low gas flow is higher, which may be due to the similar order of magnitudes between in *in situ* measurement response time and actual residual time of precursor distribution. The narrow gap is set at 500 μm with 200 sccm carrier gas flow rate. From the theory of continuous fluid in the narrow gap, separation gas flux is linearly related to precursor flux. Thus, the effective value of separation gas flow rate is also determined by the gap dimension, the carrier gas flow, and the precursor concentration.

The separation gas flow rate higher than 1000 sccm is helpful for reactant isolation, while superfluous separation flow may lead to the discontinuous distribution of precursor, resulting in a nonuniform growth. To evaluate the influence of gas flow rate on the uniformity growth, the simulations with 2500 and 5000 sccm separation gas flow rates are implemented here. Both of these separation gas flow rates are high enough for perfect reactant isolation. Growth

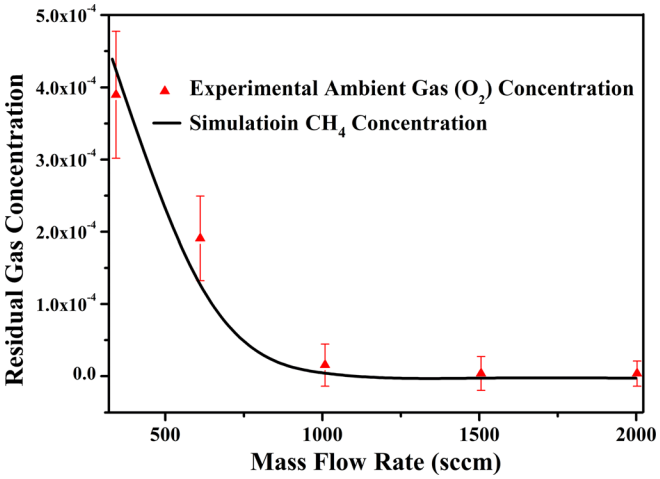

FIG. 4. (Color online) Experimental ambient gas (O_2) and simulation detection on residual species (methane) at different separation gas flow rates.

distribution perpendicular to the substrate moving direction is partitioned as zone A and B. The zones A and B locate beneath the inlet and exhaust cylinders, respectively. Growth masses at zones A and B are presented in Fig. 5(a), and the corresponding growth rates at the zone centers are shown in Fig. 5(b). The highest growth mass is 1.69×10^{-7} kg/m^2 in zone A, and the lowest growth mass is 1.57×10^{-7} kg/m^2 in zone B. The ratio of growth rates between zone A and B is about 1.07, indicating an unobvious difference in the thicknesses of the deposited film in two zones. Despite the deposition rates in zones A and B remain the same, the ratio of the regional width between the two zones decreases as the separation gas flow rate increases. When the root mean square of growth mass changes from 1.643×10^{-7} kg/m^2 at 2500 sccm to 2.047×10^{-7} kg/m^2 at 5000 sccm, the nonuniformity of the deposited film increases with higher separation gas flow rate. These numerical results of the growth uniformity are consistent with the previous reported experimental results.[16] Simulations on growth uniformity with the separation gas flow rate, carrier gas flow rate, and precursor mass fraction could be utilized to large-area substrate in the SALD system.

2. Process optimization of continuous deposition

The yield in SALD mass production is mainly characterized by the growth rate and quantity in a unit time. For the TMA and water species, the saturated surface absorption is within a few milliseconds; thus, the substrate moving speed determines the growth rate of the deposited film and the overall throughput. When the substrate moves at a constant speed, the time for saturated growth in the reaction zone is defined as the residual time. The minimal residual time will determine the maximum substrate moving speed on the precondition of uniform layer-by-layer growth. The study of the relationship between the minimal residual time and the fluid conditions is crucial to achieve a high efficiency process.

Simulations with different carrier gas flow rates and precursor mass fractions are implemented, respectively, in Figs. 6(a) and 6(b). With 1% precursor mass fraction, the minimal residual time decreases sharply with the carrier gas

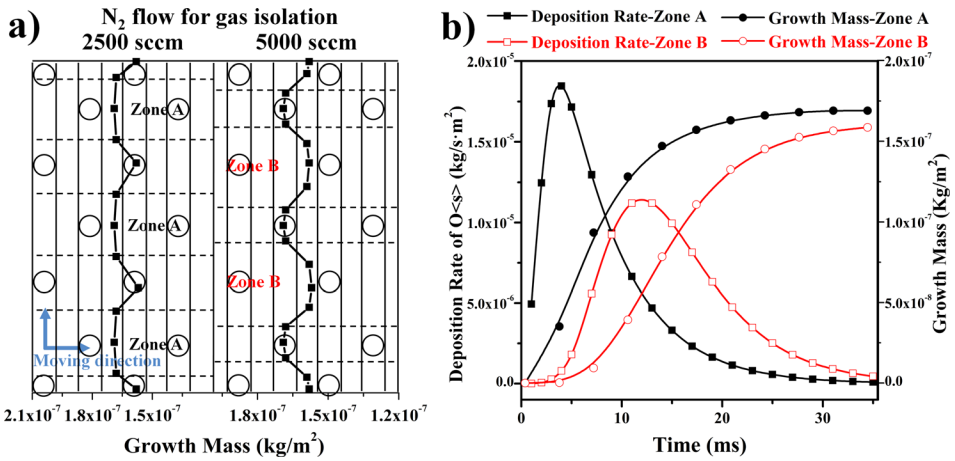

FIG. 5. (Color online) (a) Distribution of growth mass perpendicular to the direction of moving substrate; (b) deposition rates and growth rates at center of zone A and B.

flow rate increasing to 200 sccm, and then levels out even the carrier gas flow rate further increases. With the constant precursor mass fraction, higher gas flow results in larger precursor influx which may cause excess precursor for surface adsorption. Insufficient precursor dose at the carrier gas flow rate below 200 sccm leads to the unsaturated growth. In this situation, the surface growth is impacted by both the convection and the diffusion of the fluid states. With the carrier gas flow rate larger than 200 sccm, adequate precursor influx is provided at constant precursor mass fraction. When the carrier gas flow rate increases to higher than 500 sccm, the convection remains stable regardless of sufficient precursors. Therefore, the carrier gas flow is independent of the residual time improvement in the SALD system.

When the carrier gas flow rate is higher than 500 sccm, the minimal residual time is fit to the same principle with different precursor mass fractions in Fig. 6(b). With the precursor mass fraction increasing to 2%, the residual time decreases to a constant value gradually. The equilibration of the surface reaction is made with the precursor mass fraction larger than 2%. The increase of precursor concentration can improve surface reaction. The diffusion plays a dominate role when the precursor mass fraction increases at a constant carrier gas flow rate. The minimal residual time monotonously decreases with the precursor mass fraction increasing. Although the growth rate is also influenced by the substrate temperature and gas velocity, the precursor mass fraction is the dominant factor. For the high vapor pressure precursors such as TMA and Diethylzinc (DEZ), the residual time could be as short as several milliseconds with the optimum precursor mass fraction in the SALD process. Thus, compared with the growth rate of several nanometers per minute in most temporal ALD system, a growth rate obtained in SALD system could be two to three orders of magnitudes higher.

3. Precursor utilization of flow processes

As mentioned above, higher precursor concentration leads to faster growth, especially with physical adsorption of the sticking gas at atmospheric pressure. The thermal deposition above 100 °C on a planar substrate allows less physical adsorption of the molecules. The optimum usage comes from the situation that the precursor injected into reactor is completely consumed for a saturated monolayer growth. However, excess precursor concentration leads to some unreacted precursor molecules being taken away. To explore the relationship of precursor concentration and precursor

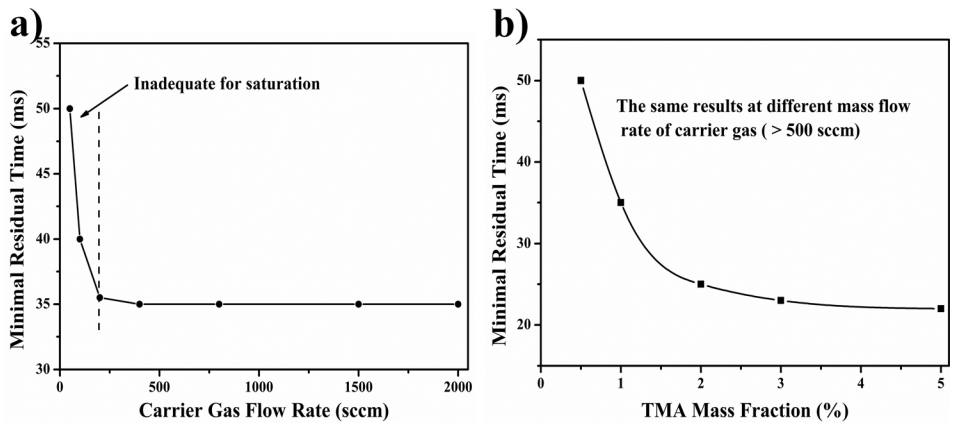

FIG. 6. (a) Minimal residual time with 1% TMA mass fraction at different carrier gas flow rates; (b) the minimal residual time with constant carrier gas flow rate at different TMA mass fractions.

utilization, the simulations on the growth rate with different TMA mass fractions are presented here. Although the residual time descends with TMA mass fractions increasing from 0.5% to 2%, the deposition rate increases steadily. As shown in Fig. 7(b), the growth rate is computed from the integral of the deposition rate with the time. When TMA mass fraction increases from 0.5% to 5%, higher growth rate is obtained as surface growth gets saturated gradually. Before surface saturation, the deposition rate will be restrained once the surface sites are fully occupied by nonreactive surface species. With the precursor concentration rising, the surface growth changes from unsaturated to a full coverage to ensure a strict self-termination growth.

The precursor usage is decided by the precursor molecules injected from inlets and the ones deposited on the surface. The comparison of precursor usage with the optimal and nonoptimal residual times is presented in Fig. 8. The optimal precursor usage and the precursor mass fraction form the monotonic decreasing relationship in the solid line. The precursor usage with a constant residual time is presented in the dotted line. When the precursor mass fraction is lower than 1%, the precursor usage maintains as high as nearly 90%. When the residual time is

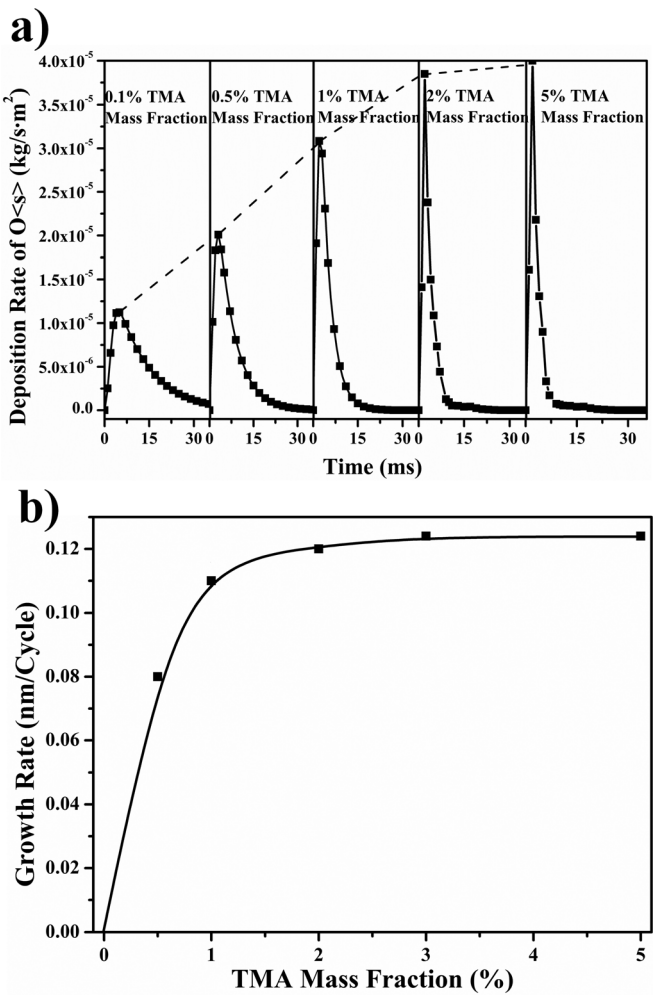

FIG. 7. (a) Deposition rates at different TMA mass fraction with constant gas flow rate; (b) the growth rates at different TMA mass fractions.

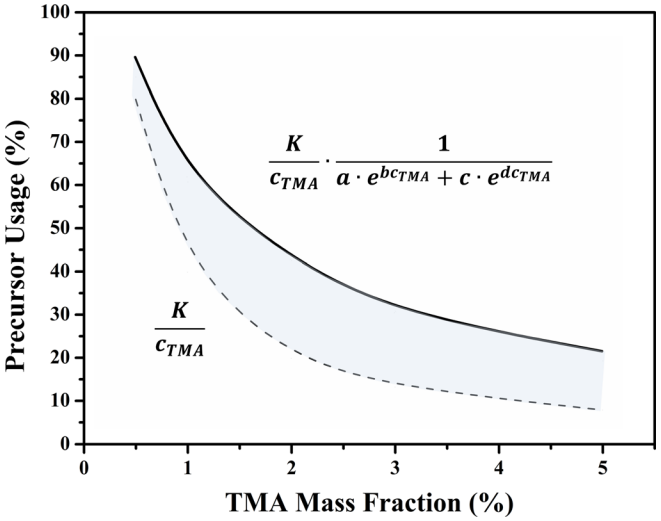

FIG. 8. (Color online) Precursor usage at different TMA mass fractions with 500 sccm carrier gas flow rate.

optimized by the method in the Sec. IV B 2, the optimal precursor usage could be obtained from summarized trend based on specific carrier gas flow rate (500 sccm) and precursor mass fractions.

With assumptions of ideal uniformity, constant thickness and constant density of the deposited film, the value of the optimum precursor usage can be calculated based on theoretical derivation. Thus, the optimum precursor usage R_{usage} in Fig. 8 could be calculated based on

$$R_{\text{usage}} = \frac{m_{\text{thin film}}}{m_{\text{flux}}} = \frac{\frac{\rho h S}{M_{\text{thin film}}} M_{\text{precursor}}}{\varphi c_p t_{\text{residual}}} = \frac{M_{\text{precursor}} \rho h S}{M_{\text{thin film}} \varphi} \cdot \frac{1}{c_p \cdot [a \cdot \exp(bc_p) + c \cdot \exp(dc_p)]}, \tag{4}$$

where $M_{\text{precursor}}$ and $M_{\text{thin film}}$ are the molar weight of precursor molecules and thin film, respectively, h is the thickness of the deposited film, S is the area of the substrate, ρ is the density of the deposited film, φ is total mass flow rate, c_p is the precursor mass fraction at inlet, t_{residual} is the minimal residual time in the precursor channel, and a, b, c, and d are all constant coefficients. Concluded from the formula (4), the precursor usage is determined by the carrier gas flow and the precursor mass fraction. The formula in solid line can be expressed as $K/c_{\text{pre}} \cdot 1/\{c_{\text{pre}} \cdot [a \cdot \exp(bc_{\text{pre}}) + c \cdot \exp(dc_{\text{pre}})]\}$ with the optimal residual time. The formula in dotted line is expressed as K/c_{pre} with 1 s unit residual time, which is a little larger than that in the reports.[14–16,19,21] Thus, the actual precursor utilization in production may stay between these two values. For the valuable precursors, low precursor mass fraction is favorable to gain better utilization by sacrificing the uniformity and the growth rate. The above theoretical analysis neglects the stickiness of precursors at atmospheric pressure which may increase the process time and limit the substrate moving speed. The substrate temperature is heated to 150 °C to improve the precursor stickiness. The sticking coefficient is assumed unitive

considering the simple adsorption/desorption processes and the direct pathway for species transport on the planar substrate. Overall processes above base on Al_2O_3 thin film with TMA and water as precursors. If other precursors and films are involved, it is necessary to find out the corresponding surface adsorption coefficient, chemical reactions, and fluid properties. For example, the nanolaminates of zinc oxide and titanium oxide can be analyzed with the independent modeling, and then, the simulation results are stacked together.

From the above discussion, the precursor concentration is the major parameters in the optimization of the minimal residual time. The Péclet number measures the interaction between the convection and the diffusion in precursor transport. As the moving substrate is sequentially exposed to reaction/separation zones, the deposition process in each reaction zone could be considered as an elementary unit for fluid kinetics analysis. From fundamental fluid dynamics theory presented in the Appendix, formula (A4)–(A6), the axial velocity and the diffusion coefficient are calculated specifically with the substrate temperature, the pressure, the mass flow rate, and the characteristic length. The characteristic length in the SALD system is usually less than 1 mm, which is an order of magnitude smaller than that in temporal ALD system. Due to the low Péclet number, the diffusion transport far outweighs the convection. Results of computational modeling reveal the important role of the diffusion in precursor transport, which could be generalized to incorporate other SALD systems with different structures.

V. SUMMARY AND CONCLUSIONS

A numerical model for atmospheric SALD process is presented in this paper. By coupling with volumetric reactions on reactant isolation, the film growth throughput and precursor utilization can be quantitatively simulated. The effect of separation gas flow rate, carrier gas flow rate, and precursor mass fraction is discussed, respectively. The separation gas flow rate deduced from our numerical SALD model agrees well with the experimental ones, which validate the feasibility of this model. From the simulation results, the precursor concentration is the determinant factor of the minimal residual time. The overall throughput of the film deposition is determined by the minimal residual time. The optimum precursor usage of the continuous process is inversely proportional to the carrier gas flow rate. With a constant carrier gas flow, the optimal precursor usage and the precursor mass fraction form a monotonic decreasing relationship. The gap between the gas head and the substrate, regardless of its specific structures in any SALD system, leads to a low Péclet number, which place the diffusion in a leading role in precursor transport rather than convection. The methodology of combing experiments and simulations could be utilized to optimize the film growth by other reactants, and would be informative for process optimization as well as system structure design.

ACKNOWLEDGMENTS

The authors would like to acknowledge Aoming Li from AMETEK lab for mass spectrum detection, as well as technology support by the Analytic Testing Center of HUST. This work was supported by the National Basic Research Program of China (2013CB934800), the National Natural Science Foundation of China (51575217 and 51572097), and the Hubei Province Funds for Distinguished Young Scientists (2015CFA034 and 2014CFA018). Rong Chen acknowledges the Thousand Young Talents Plan, the Recruitment Program of Global Experts, and the Program for Changjiang Scholars and Innovative Research Team in University (IRT13017).

APPENDIX

Besides of chemical reactions in formula (2) and (3), typical ALD process is also decoupled into several physical procedures, mass transfer, momentum transport, and convective heat transfer. Each procedure is governed by corresponding partial differential equations, which can be solved numerically on the defined domain. The continuum-based finite volume method assumes the concerned domain as a continuum. Thus, the continuity equation conserves mass

$$\frac{\partial \rho}{\partial t} + \nabla \cdot (\rho \boldsymbol{V}) = 0, \tag{A1}$$

where ρ is the density and $\boldsymbol{V}$ is the velocity vector. The process of momentum transport within the laminar flow in the ALD chamber is governed by the momentum conservation equation

$$\frac{\partial}{\partial t}(\rho \boldsymbol{V}) + \nabla \cdot (\rho \boldsymbol{V}\boldsymbol{V}) + \nabla \cdot \tau = F, \tag{A2}$$

where F is external body forces and τ is the stress tensor. To model the species transport in ALD system, the convection–diffusion equation is adopted, which takes the following form:

$$\frac{\partial}{\partial t}(\rho c_i) + \nabla \cdot (\rho \boldsymbol{V} c_i) = -\nabla \cdot \boldsymbol{J}_i + S_i, \tag{A3}$$

where c_i is the local molar fraction of species i, R_i is the net rate of production of species i by chemical reaction, and S_i is the source term.

From fluid theory, The Péclet number defines the relative importance of convection to diffusion transport and fits the following equation:

$$Pe = \frac{vL}{\alpha}, \tag{A4}$$

where v is the average gas velocity, L is the characteristic length, and α is the diffusion coefficient. The average gas velocity, that is, the bulk stream velocity U_∞, can be deduced from the formula of flow conductivity and presented with the mass flow rate and pressure through the following equation:

$$U_\infty = \frac{P_0}{P}\frac{T}{T_0}\frac{4\varphi}{\pi d^2}, \tag{A5}$$

where the bulk stream velocity is parallel to the substrate, P, T, and φ are the pressure, chamber temperature, and mass flow rate, respectively. P_0 and T_0 are, respectively, the atmospheric pressure and room temperature. On the other hand, the diffusion coefficient can be determined using the Chapman–Engskov approximation

$$D_{A-B} = \frac{3CkT}{8P}\sqrt{\frac{kT}{2\pi}\left(\frac{1}{M_A}+\frac{1}{M_B}\right)}, \tag{A6}$$

where M_A and M_B are the molecular mass of precursor and carrier gas, C is a constant which depends on the precursor–carrier gas interaction potential, P is the pressure, k is the Boltzmann constant, and T is the temperature (K). Diffusion coefficient is just inversely proportional to the pressure. Thus, the Péclet number in the SALD depends mainly on the gap dimension and the mass flow rate.

[1]S. M. George, Chem. Rev. **110**, 111 (2010).
[2]R. L. Puurunen, J. Appl. Phys. **97**, 121301 (2005).
[3]W. M. M. Kessels and M. Putkonen, MRS Bull. **36**, 907 (2011).
[4]R. L. Puurunen, Chem. Vap. Deposition **9**, 249 (2004).
[5]R. L. Puurunen and W. Vandervorst, J. Appl. Phys. **96**, 7686 (2004).
[6]E. Granneman, P. Fischer, D. Pierreux, H. Terhorst, and P. Zagwijn, Surf. Coat. Technol. **201**, 8899 (2007).
[7]J. C. S. Kools, Electrochem. Soc. Trans. **41**, 195 (2011).
[8]M. B. M. Mousa, C. J. Oldham, J. S. Jur, and G. N. Parsons, J. Vac. Sci. Technol. A **30**, 01A155 (2012).
[9]J. S. Jur and G. N. Parsons, ACS Appl. Mater. Interfaces **3**, 299 (2011).
[10]M. B. M. Mousa, C. J. Oldham, and G. N. Parsons, Langmuir **30**, 3741 (2014).
[11]P. Poodt, D. C. Cameron, E. Dickey, S. M. George, V. Kuznetsov, G. N. Parsons, F. Roozeboom, G. Sundaram, and A. Vermeer, J. Vac. Sci. Technol. A **30**, 010802 (2012).
[12]A. Illiberi, R. Scherpenborg, Y. Wu, F. Roozeboom, and P. Poodt, ACS Appl. Mater. Interfaces **5**, 13124 (2013).
[13]D. H. Levy, D. Freeman, S. F. Nelson, P. J. Cowdery-Corvan, and L. M. Irving, Appl. Phys. Lett. **92**, 192101 (2008).
[14]D. H. Levy, S. F. Nelson, and D. Freeman, J. Disp. Technol. **5**, 484 (2009).
[15]D. H. Levy and S. F. Nelson, J. Vac. Sci. Technol. A **30**, 018501 (2012).
[16]P. R. Fitzpatrick, Z. M. Gibbs, and S. M. George, J. Vac. Sci. Technol. A **30**, 01A136 (2012).
[17]K. Sharma, R. A. Hall, and S. M. George, J. Vac. Sci. Technol. A **33**, 01A132 (2015).
[18]P. Poodt, A. Lankhorst, F. Roozeboom, K. Spee, D. Maas, and A. Vermeer, Adv. Mater. **22**, 3564 (2010).
[19]P. Poodt, A. Illiberi, and F. Roozeboom, Thin Solid Films **532**, 22 (2013).
[20]P. Poodt, R. Knaapen, F. Roozeboom, and A. van Asten, J. Vac. Sci. Technol. A **30**, 01A142 (2012).
[21]P. S. Maydannik, T. O. Kääriäinen, and D. C. Cameron, Chem. Eng. J. **171**, 345 (2011).
[22]P. S. Maydannik, T. O. Kääriäinen, and D. C. Cameron, J. Vac. Sci. Technol. A **30**, 01A122 (2012).
[23]K. Ali, K. H. Choi, J. Jo, and Y. W. Lee, Mater. Lett. **136**, 90 (2014).
[24]E. Dickey and W. A. Barrow, J. Vac. Sci. Technol. A **30**, 021502 (2012).
[25]P. S. Maydannik *et al.*, J. Vac. Sci. Technol. A **32**, 051603 (2014).
[26]A. S. Yersak, Y. C. Lee, J. A. Spencer, and M. D. Groner, J. Vac. Sci. Technol. A **32**, 01A130 (2014).
[27]F. J. van den Bruele, M. Smets, A. Illiberi, Y. Creyghton, P. Buskens, F. Roozeboom, and P. Poodt, J. Vac. Sci. Technol. A **33**, 01A131 (2015).
[28]M. Aghaee, P. S. Maydannik, P. Johansson, J. Kuusipalo, M. Creatore, T. Homola, and D. C. Cameron, J. Vac. Sci. Technol. A **33**, 041512 (2015).
[29]P. Poodt, J. van Lieshout, A. Illiberi, R. Knaapen, F. Roozeboom, and A. van Asten, J. Vac. Sci. Technol. A **31**, 01A108 (2013).
[30]A. Yanguas-Gil and J. W. Elam, J. Vac. Sci. Technol. A **32**, 031504 (2014).
[31]Y. Y. Xie, L. L. Ma, D. Q. Pan, and C. Yuan, Chem. Eng. J. **259**, 213 (2015).
[32]M. R. Shaeri, T. C. Jen, and C. Y. Yuan, Int. J. Heat Mass Trans. **78**, 1243 (2014).
[33]D. Q. Pan, L. L. Ma, Y. Y. Xie, T. C. Jen, and C. Yuan, J. Vac. Sci. Technol. A **33**, 021511 (2015).